International Journal of Precision Engineering and Manufacturing (2020) 21:895–904
https://doi.org/10.1007/s12541-019-00306-7

Online ISSN 2005-4602
Print ISSN 2234-7593

REGULAR PAPER

Analytical Compliance Model for Right Circle Flexure Hinge Considering the Stress Concentration Effect

Weixiao Tuo[1] · Xingfei Li[1] · Yue Ji[2] · Tengfei Wu[1] · Ziming Xie[1]

Received: 31 May 2019 / Revised: 21 November 2019 / Accepted: 25 December 2019 / Published online: 14 January 2020

Abstract

In this paper, an analytical compliance model for right circle flexure hinge (RCFH) is presented with the stress concentration in consideration. The stress concentration caused by changes in RCFH's cross-section usually happens at the weakest point. It has been shown to seriously affect RCFH's compliance calculation. Based on the virtual work theory, superposition relationship of the deformation, as well as Castigliano's second theorem, RCFH's analytical compliance model considering the stress concentration effect is established. The model is calculated as a series of closed-form equations which are related with geometric dimensions and employed material. Complicated definite integrals existing in these compliance equations are proved to be correctly calculated through comparisons with other literatures. Finally, in order to examine the validity of the established model, finite element analysis (FEA) is conducted. The relative errors between the theoretical values obtained by the established model and FEA results are found within 20% for a wide range of geometric dimensions.

Keywords Right circle flexure hinge · Compliance model · Stress concentration · Finite element analysis

1 Introduction

Flexure hinges are frequently designed to transmit the relative motion between adjacent rigid links through elastic deformation [1]. Unlike conventional revolute joints, flexure hinges are free of friction and lubrication, capable of smooth motion and infinite resolution, and moreover, almost insusceptible to temperature [2]. Thus, flexure hinges are commonly used in many applications including micro-position platform [3, 4], micro-gripper [5], and micro-electro-mechanical systems (MEMS) [6]. Among various flexure hinges, cycloidal and filleted V-shaped flexure hinge were proved to possess higher rotational precision than RCFH [7, 8]. However, RCFH has a broader range of applications where high positioning accuracy and resolution are required [9, 10]. This is mainly due to its convenience and readily available machining processes. When RCFH is integrated in a mechanism, the static and dynamic characteristics of the system mainly depend on RCFH's behaviors [11]. As one of the most important performance indexes, compliance of RCFH needs to be accurately modeled to reduce the modeling errors.

Analytical modeling and FEA are the two most commonly used approaches in RCFH's compliance modeling. The compliances of RCFH obtained by FEA are always more accurate with respect to experimental data [12, 13]. However, FEA lacks of physical meaning and cannot construct the analytical relationship between the applied loads and resulting deformations. Moreover, the fine meshes achieving high precision usually result in massive computations [14]. In contrast, analytical modeling can provide a set of optimized design parameters in less time. Therefore, analytical modeling is preferred for the dimension synthesis during the design and optimization stage.

Starting with Paros and Weisbord's seminal work as early as 1965 [15], various analytical solutions for RCFH's compliance have been provided. With some exceptions [16, 17], most of them are based on the assumption of small deformation due to RCFH's relatively low compliance and wide applications in small displacement-oriented systems [18]. Paros and Weisbord [15] presented both exact and tractable simplified closed-form equations for RCFH. The angular and

✉ Xingfei Li
lixftju@hotmail.com

[1] State Key Laboratory of Precision Measuring Technology and Instruments, Tianjin University, Tianjin 300072, China

[2] Key Laboratory of Advanced Electrical Engineering and Energy Technology, Tianjin Polytechnic University, Tianjin 300387, China

linear compliances for bending and axial loads were developed based on the theory of mechanics of materials. Wu and Zhou [19] utilized the integration of linear differential equations and provided a set of more concise closed-form equations. Their equations were proved to have the same percentage errors as Paros and Weisbord's exact equations (neglecting signs). Lobontiu [1] developed the in-plane and out-of-plane compliances of RCFH based on the Castigliano's second theorem. During modeling RCFH's torsional compliance, the thick-to-width ratio of the cross-section was supposed to be equal to or larger than 1 (or equal to or less than 1) for the whole notch region [20]. Tseytlin [21] adopted the inverse conformal mapping method to predict the rotational compliance of RCFH. The predictions were likely to be much closer to FEA results and experimental data. Afterwards, Yong et al. [22] compared the previously reviewed models with FEA results. A guideline for selecting the most suitable and accurate compliance equations for RCFH was presented. Chen and Howell [23] also summarized preexisting equations for RCFH's torsional compliance and analyzed their computational accuracy. Two new equations were proposed, which were independent to the relative magnitude of the cross-sectional thickness and width. However, the equation that Chen and Howell adopted for the torsional moment of inertia was in terms of the rectangular beam with constant cross-section [24], which will result in inevitable errors. Xu et al. [25] divided RCFH into a series of rectangular section unit beams and developed an analytical model for RCFH based on the theory of elasticity and infinitesimal method. Larger number of unit beams usually corresponds to higher accuracy and worse computational efficiency.

The thorough review of RCFH's analytical compliance models has indicated that there are no analytical compliance models for RCFH with the stress concentration in consideration. However, the stress concentration has been proved to have significant influence on RCFH's compliance calculation [22, 26]. In addition, preexisting equations calculating torsional compliance for RCFH with any dimensions were not available. Thus, this paper presents an analytical compliance model for RCFH, which takes the stress concentration into account. The established model is expected to be helpful in automating the design of RCFH and better understanding its behavior.

The remainder of this paper is organized as follows. In Sect. 2, RCFH's geometric as well as generic compliance model are presented firstly. Then, using FEA, the effect of stress concentration on RCFH is analyzed. Finally, modeling method with the stress concentration in consideration are presented. The in-plane and out-of-plane compliances of RCFH are calculated as a series of closed-form equations related with geometric dimensions and employed material in Sect. 3. Comparisons with other literatures and FEA are conducted in Sect. 4 to verify the established model. Finally, the paper ends with a conclusion in Sect. 5.

2 Compliance Model

2.1 Generic Compliance Model

RCFH is usually fabricated by removing two symmetric round cutouts from the rectangular beam. Thus, it is composed of two parts, the circle notch region and rigid beams. The boundary conditions of RCFH are acceptable to be fixed-free, which has been the case with all analytical approaches to RCFH ever since the work of Paros and Weisbord [15]. Figure 1 illustrates a fixed-free generic RCFH subjected to three-dimensional loads at its free end. The three-dimensional loads are defined as the loading vector $\{L\} = \left[F_x, F_y, F_z, M_x, M_y, M_z\right]^T$, including two bending moments M_y, M_z, two shearing forces F_y, F_z, one axial force F_x, and one torsional moment M_x. The resulting deformations are described as the deformation vector $\{\delta\} = \left[u_x, u_y, u_z, \theta_x, \theta_y, \theta_z\right]^T$, including three translations u_x, u_y, u_z, and three rotations $\theta_x, \theta_y, \theta_z$. Geometric definitions of RCFH are illustrated in Fig. 1 as well, mainly including the cutting radius r, the minimum thickness t, and the depth w. The Cartesian coordinate system is utilized, where the origin is located at the midpoint of the free end, and the x-, y- and z-axes are the longitudinal, altitudinal and depth directions, respectively.

Due to RCFH's relatively low compliance and wide applications in small displacement-oriented systems, this work mainly focuses on RCFH whose deformations are small (infinitesimal). Thus, the small deformation theory can be applied and the geometrically nonlinear effect can be neglected [27]. In addition, the parasitic motion is ignored in this work because it could be reduced to be negligible with some precautions [28, 29]. Then, the deformation vector $\{\delta\}$, loading vector $\{L\}$ and the compliance matrix [C] of RCFH can be connected by Hooke's law, namely $\{\delta\} = [\mathrm{C}]\{L\}$ with

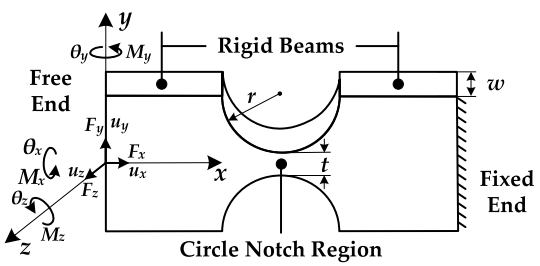

Fig. 1 Boundary conditions, geometric parameters, spatial loads and resulting deformations of a generic RCFH

$$[C] = \begin{bmatrix} C_{u_x-F_x} & 0 & 0 & 0 & 0 & 0 \\ 0 & C_{u_y-F_y} & 0 & 0 & 0 & C_{u_y-M_z} \\ 0 & 0 & C_{u_z-F_z} & 0 & C_{u_z-M_y} & 0 \\ 0 & 0 & 0 & C_{\theta_x-M_x} & 0 & 0 \\ 0 & 0 & C_{\theta_y-F_z} & 0 & C_{\theta_y-M_y} & 0 \\ 0 & C_{\theta_z-F_y} & 0 & 0 & 0 & C_{\theta_z-M_z} \end{bmatrix} \quad (1)$$

The subscript pair of any compliance in Eq. (1) corresponds to the deformation at the free end and the particular load producing that deformation. According to Maxwell's reciprocity principle, following equations can be yielded

$$C_{u_z-M_y} = C_{\theta_y-F_z}, C_{u_y-M_z} = C_{\theta_z-F_y} \quad (2)$$

which indicates that [C] is a symmetric square matrix.

2.2 Influence of Stress Concentration

Due to its high accuracy, FEA is usually regarded as a reliable method to estimate RCFH's behaviors. The stress and strain obtained by FEA are always accurate with respect to experimental data. Therefore, FEA is conducted here to simulate RCFH's stress and strain. During the numerical calculations, geometric parameters of RCFH are given as $r = 5$ mm, $t = 1$ mm, and $w = 5$ mm. Details about FEA settings are demonstrated in Sect. 4.2.

It can be observed from Fig. 2 that the iso-strain and iso-stress plane are not perpendicular to the x-axis either parallel to each other when RCFH is subjected to a unit axial load F_x. This is not consistent with theoretical assumptions and mainly because of the stress concentration happening at RCFH's weakest point.

In order to obtain a clear view, FEA results as well as theoretical deformations along a selected path are compared in Fig. 3. The path origins from the center of the fixed end and ends at the center of the free end, as depicted in Fig. 3a.

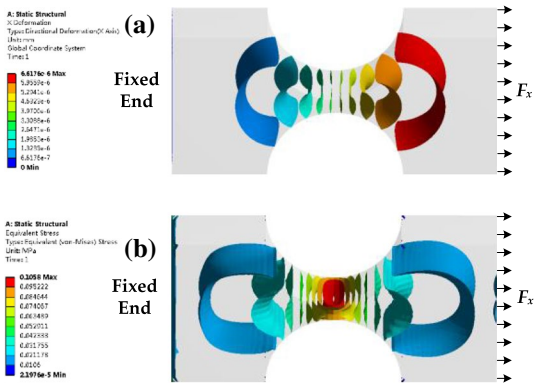

Fig. 2 FEA results of RCFH's stress and strain distributions; **a** Iso-strain plane, **b** iso-stress plane

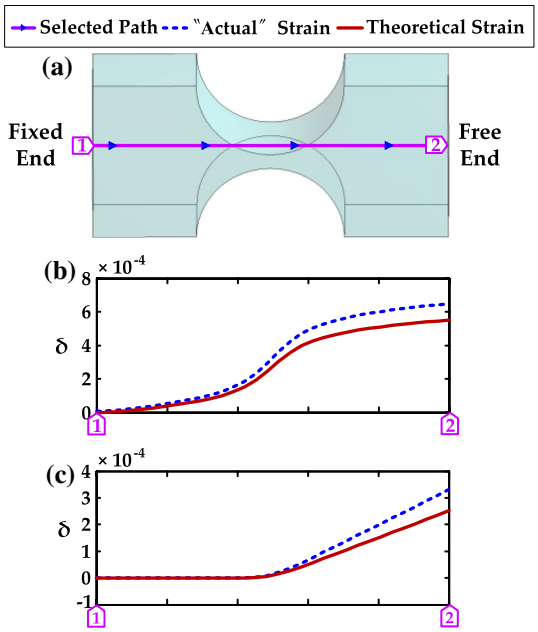

Fig. 3 Comparisons between FEA results and theoretical values; **a** definition of the selected path, **b** deformations for a unit axial force, **c** deformations for a unit bending moment

According to the results plotted in Fig. 3b and c, it is clear that RCFH's deformations obtained by FEA are slightly larger than the theoretical values either for a unit axial force or a bending moment. This phenomenon indicates that the stress concentration has significant influence on RCFH's compliance calculation. Therefore, more attentions must be directed towards the stress concentration effect within RCFH as well as RCFH-based mechanisms designs to reduce modeling errors.

2.3 Modeling Method

From the qualitative analyses above and Saint–Venant's principle, it is noted that the stress concentration only affects the region near the circle notch. For the sake of generality, RCFH with two relatively long beam connections is considered in this work, which can be regarded as a flexure serial chain that is formed with five flexure members, as depicted in Fig. 4.

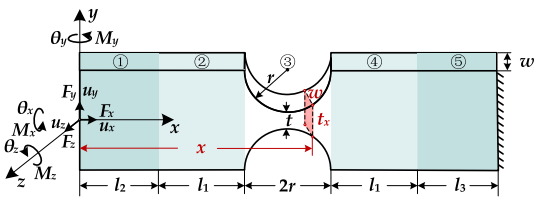

Fig. 4 RCFH with two relatively long beam connections

It is expected that the stress concentration only affects the second and forth segments and has little effect on the first and fifth segments. Compared to RCFH illustrated in Fig. 1, the configuration of Fig. 4 adds another three design parameters, the length of beam connections near to the circle notch l_1, and the length of beam connections far away from the circle notch on both sides l_2, l_3. Based on the virtual work theory and the superposition relationship of the deformation, the overall compliance matrix of RCFH [C] can be expressed as

$$[\mathrm{C}] = \sum_{i=1}^{5} [J_i] \cdot [\mathrm{C}_i] + [\mathrm{C}_s] \tag{3}$$

where $[J_i]$ means the transformation matrix, $[\mathrm{C}_i]$ stands for the compliance matrix of the segment i, $[\mathrm{C}_s]$ represents for the additional compliance caused by the stress concentration. The transformation matrix comes in the following form

$$[J_i] = \begin{bmatrix} [R_i] & 0_{4\times 2} \\ 0_{2\times 4} & N_i \cdot [S_i] \end{bmatrix} \tag{4}$$

where $[R_i]$, $[S_i]$ are 4×4, 2×2 unit square matrix, respectively. N_i is the mapping coefficient and there are

$$\begin{cases} N_1 = l_1/l \\ N_2 = (l_1 + l_2)/l \\ N_3 = (l_1 + l_2 + 2r)/l \\ N_4 = (2l_1 + l_2 + 2r)/l \\ N_5 = 1 \end{cases} \tag{5}$$

where l is the total length of the specimen and equal to $2l_1 + l_2 + l_3 + 2r$. According to the results of Li et al. [26], $[\mathrm{C}_s]$ can be equivalent to the compliance of a rectangular beam that locates at the same position with the circle notch. The length, width and height of the rectangular beam are $2r$, $2r + t$, and w, respectively. Then, Eq. (3) can be reformulated as

$$[\mathrm{C}] = [\mathrm{C}_r] + [J_3] \cdot [\mathrm{C}_3] \tag{6}$$

where $[\mathrm{C}_r]$, $[\mathrm{C}_3]$ are the compliance matrices of the rectangular beam over the whole RCFH and the circle notch region, respectively. Without loss of generality, two new variables h_1 and h_2 are introduced to substitute for $l_1 + l_2$ and $l_1 + l_3$, respectively, which will make Eq. (6) universal to RCFH with short beam connections.

3 Analytical Compliance Model

According to the analysis in Sect. 2.3, the main requirement for RCFH's compliance model is to solve the compliance matrixes of the rectangular beam over the whole RCFH and the circle notch region. In this section, both of them are analytically calculated.

3.1 Compliance Matrix of the Rectangular Beam

The rectangular beam with constant cross-section has been overwhelmingly investigated. Meanwhile, the established compliance models have been proved to be precise for most practical applications. Therefore, the compliance matrix of the rectangular beam over the whole RCFH can be directly given as

$$[\mathrm{C}_r] = \begin{bmatrix} \frac{l}{Ews} & 0 & 0 & 0 & 0 & 0 \\ 0 & \frac{\alpha l}{Gws} + \frac{4l^3}{Ews^3} & 0 & 0 & 0 & \frac{6l^2}{Ews^3} \\ 0 & 0 & \frac{\alpha l}{Gws} + \frac{4l^3}{Ew^3 s} & 0 & -\frac{6l^2}{Ew^3 s} & 0 \\ 0 & 0 & 0 & \frac{l}{GI_t} & 0 & 0 \\ 0 & 0 & -\frac{6l^2}{Ew^3 s} & 0 & \frac{12l}{Ew^3 s} & 0 \\ 0 & \frac{6l^2}{Ews^3} & 0 & 0 & 0 & \frac{12l}{Ews^3} \end{bmatrix} \tag{7}$$

where s is an intermediate variable and equal to $2r + t$. E and G are the Young's modulus and the shear modulus, respectively. α is the shear coefficient and commonly equal to 6/5 for a rectangular cross-section. $\mathrm{I_t}$ is the torsional moment of inertia. For a rectangular cross-section with the length of h and width of b, I_t can be expressed as $\beta h b^3$, where β is the torsional shape coefficient. The representative corresponding values of the length–width ratio k and β are available in Table 1.

However, it is worth mentioning that these discrete values are often inadequate for engineering design. In order to satisfy the practical applications, approximate continuous equations for the torsional shape coefficient were

Table 1 Representative corresponding values of k and β

k	β
1.0	0.141
1.2	0.166
1.5	0.196
2.0	0.229
2.5	0.249
3.0	0.263
4.0	0.281
6.0	0.299
8.0	0.307
10.0	0.313
50.0	0.329
∞	1/3

in demand, which has been provided by Hearn [24] and Young [30]. Their equations are given as

$$\beta_{\mathrm{H}} = \frac{k^2}{3.5k^2 + 3.5}, \quad \beta_{\mathrm{Y}} = \frac{1}{3} - \frac{0.21}{k}\left(1 - \frac{1}{12k^4}\right) \tag{8}$$

where β_{H} indicates Hearn's equation and β_{Y} indicates Young's equation. In order to know which equation is more accurate, β_{H}, β_{Y}, as well as representative corresponding values of β are compared together in Fig. 5. It is apparent that β_{Y} is more consistent with those discrete values listed in Table 1. Therefore, β_{Y} is adopted here, and two cases for calculating I_t are summarized in Table 2.

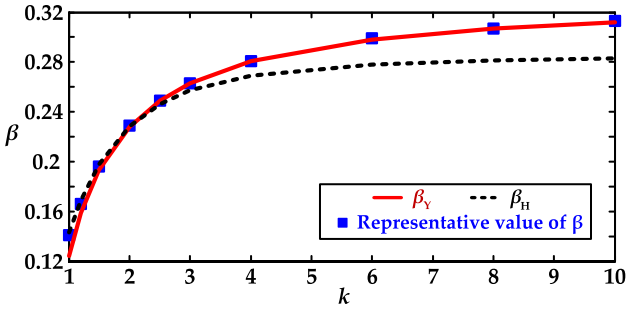

Fig. 5 Descriptions of representative values of β, as well as continuous equations β_{H} and β_{Y}

Table 2 Two cases for calculating I_t

Conditions	I_t
$2r + t > w$	$w^3(2r+t)\left[\frac{1}{3} - 0.21\frac{w}{2r+t}\left(1 - \frac{w^4}{12(2r+t)^4}\right)\right]$
$2r + t < w$	$(2r+t)^3 w\left[\frac{1}{3} - 0.21\frac{2r+t}{w}\left(1 - \frac{(2r+t)^4}{12w^4}\right)\right]$

3.2 Compliance Matrix of the Circle Notch Region

In order to derive closed-form compliance equations for the circle notch region, the Castigliano's second theorem is adopted and written as

$$\Delta = \frac{\partial U}{\partial P} \tag{9}$$

where Δ is the deformation due to the applied load, U is the strain energy stored, and P is the applied load. The strain energy is determined by the applied loads and expressed as

$$U = \int_{h_1}^{h_1+2r} \frac{F_x^2}{2EA} + \frac{\alpha F_y^2}{2GA} + \frac{\alpha F_z^2}{2GA} + \frac{M_x^2}{2GJ_x} + \frac{\left(M_y + xF_z\right)^2}{2EI_y} + \frac{\left(M_z + xF_y\right)^2}{2EI_z} dx \tag{10}$$

where I_y, I_z are cross-sectional moments of the area in the y and z direction and equal to $w^3 t_x/12$ and $w t_x^3/12$, respectively. A is the cross-sectional area. J_x is the torsional moment of inertia for the infinitesimal strip dx at position x. The variational thickness t_x can be expressed as

$$t_x = t + 2\left[r - \sqrt{2r(x - h_1) - (x - h_1)^2}\right] \tag{11}$$

Then, the linear and angular compliances except for torsional compliance can be easily derived. Concrete expressions of these compliances and f_i ($i = 1$–4) involved are expressed as follows:

$$[\mathrm{C}_3] = \begin{bmatrix} \frac{1}{Ew}f_1 & 0 & 0 & 0 & 0 & 0 \\ 0 & \frac{\alpha}{Gw}f_1 + \frac{12}{Ew}f_2 & 0 & 0 & 0 & \frac{12(r+h_1)}{Ew}f_4 \\ 0 & 0 & \frac{\alpha}{Gw}f_1 + \frac{12}{Ew^3}f_3 & 0 & -\frac{12(r+h_1)}{Ew^3}f_1 & 0 \\ 0 & 0 & 0 & \frac{1}{G}\int_{h_1}^{h_1+2r}\frac{1}{J_x}dx & 0 & 0 \\ 0 & 0 & -\frac{12(r+h_1)}{Ew^3}f_1 & 0 & \frac{12}{Ew^3}f_1 & 0 \\ 0 & \frac{12(r+h_1)}{Ew}f_4 & 0 & 0 & 0 & \frac{12}{Ew}f_4 \end{bmatrix} \tag{12}$$

$$f_1 = -\frac{\pi}{2} + \frac{2(2r+t)}{\sqrt{t(4r+t)}}\arctan\sqrt{\frac{4r+t}{t}} \tag{13}$$

$$f_2 = \frac{96r^3\left(h_1+r\right)^2 + 32r^2\left(2h_1^2+4rh_1+3r^2\right)t + 8r\left(2h_1^2+4rh_1+(11+4\pi)r^2\right)t^2 + 32(1+\pi)r^2t^3}{8t^2(2r+t)(4r+t)^2} + \frac{2(2+5\pi)rt^4+\pi t^5}{8t^2(2r+t)(4r+t)^2} + \frac{4(2r+t)\left(24r^2\left(h_1+r\right)^2+8r^3t-14r^2t^2-8rt^3-t^4\right)arctan\sqrt{\frac{4r+t}{t}}}{8t^{5/2}(4r+t)^{5/2}} \tag{14}$$

$$f_3 = -\frac{1}{2}\pi h_1^2 - \pi r h_1 - \frac{1}{4}(-4+\pi)r^2 + \frac{1}{2}(1+\pi)rt + \frac{1}{8}\pi t^2 + \frac{4(2r+t)\left(4\left(h_1+r\right)^2-4rt-t^2\right)arctan\sqrt{\frac{4r+t}{t}}}{8\sqrt{t(4r+t)}} \tag{15}$$

$$f_4 = \frac{2r\left(t(4r+t)\left(6r^2+4rt+t^2\right)+6r(2r+t)^2\sqrt{t(4r+t)}arctan\sqrt{\frac{4r+t}{t}}\right)}{t^3(2r+t)(4r+t)^3} \tag{16}$$

According to Sect. 3.1, β_Y is considered to be more accurate than β_H, therefore, there should be

$$J_x = \begin{cases} \beta_Y w^3 t_x & t_x \geq w \\ \beta_Y w t_x^3 & t_x < w \end{cases} \tag{17}$$

However, the high-order term existing in β_Y makes Eq. (17) difficult to integral. In terms of that, a more simplified equation $\beta_L = 0.333 - 0.21/k$ proposed by Lobontiu et al. [20] is adopted. The Root Mean Square Error (RMSE) of β_Y, β_L and β_H are calculated, which are 0.006, 0.0063 and 0.015, respectively. This indicates that β_L is more suitable for applications where high computational accuracy and efficiency need to be achieved simultaneously. Then, three cases for calculating C_{3,θ_x-M_x} are listed in Table 3 where β_L is adopted.

Table 3 Three cases for calculating C_{3,θ_x-M_x}

Conditions	C_{3,θ_x-M_x}
$2r+t<w$	$\frac{1}{G}\int_{h_1}^{h_1+2r}\frac{1}{wt_x^3/3-0.21t_x^4}dx$
$t<w\leq 2r+t$	$\frac{1}{Gw^3}\int_{h_1}^{p_1}\frac{1}{t_x/3-0.21w}dx + \frac{1}{G}\int_{p_1}^{p_2}\frac{1}{wt_x^3/3-0.21t_x^4}dx + \frac{1}{Gw^3}\int_{p_2}^{h_1+2r}\frac{1}{t_x/3-0.21w}dx$
$w<t$	$\frac{1}{Gw^3}\int_{h_1}^{h_1+2r}\frac{1}{t_x/3-0.21w}dx$

$p_1 = h_1 + r - \frac{\sqrt{(w-t)(4r+t-w)}}{2}$, $p_2 = h_1 + r + \frac{\sqrt{(w-t)(4r+t-w)}}{2}$

4 Comparisons and FEA Validation

4.1 Comparisons

It should be pointed out that there are many definite integrals in the compliance equations of the circle notch region. In order to verify these mathematic relationships, comparisons are conducted between the model established in Sect. 3.2 (donated by Tuo) and other preexisting ones, mainly including Paros and Weisbord's (both full and simplified, donated by Paros (full) and Paros (Simp.), respectively), Wu and Zhou's (donated by Wu), Lobontiu's (donated by Lo.), Tseytlin's, as well as Chen's. For all comparisons, Titanium alloy (Tc4) is chosen as the linearly elastic material. The properties of Tc4 are: Young's modulus $E = 110$ GPa, Poisson's ratio $\nu = 0.34$, shear modulus $G = 43$ GPa, and density $\rho = 4500\,\mathrm{kg/m^3}$. The width w and thickness t of all compared right circle flexure hinges (RCFHs) are chosen as 10 mm and 1 mm, respectively. The results are depicted in Fig. 6, where r varies from 0.5 to 10.

From Fig. 6, following points can be easily drawn:

- Results of Wu and Tuo are identical when considering the shear effect. Due to its high accuracy and wide applications, Wu's model is usually regarded as a reliable solution for RCFH's compliance. Thus, the mathematic relationships in Sect. 3.2 can be considered correct. However, the equation calculating RCFH's torsional compliance was not mentioned in Wu's work.
- Torsional compliance calculated by Tuo's model has the same trend with Chen's results. However, the differ-

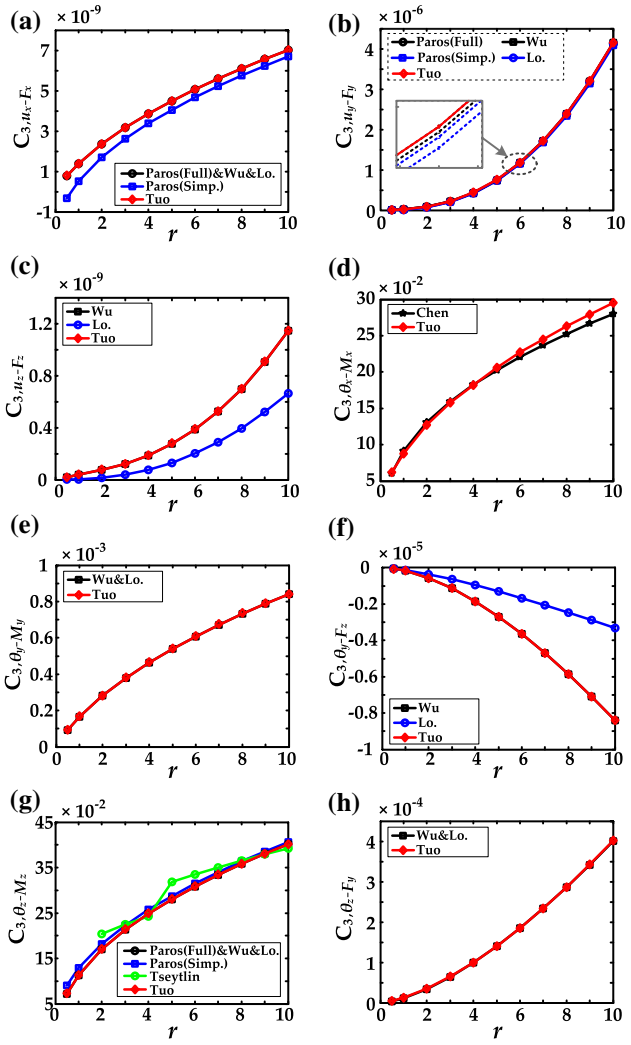

Fig. 6 Comparisons with other analytical compliance models for the circle notch region; **a** C_{3,u_x-F_x}, **b** C_{3,u_y-F_y}, **c** C_{3,u_z-F_z}, **d** C_{3,θ_x-M_x}, **e** C_{3,θ_y-M_y}, **f** C_{3,θ_y-F_z}, **g** C_{3,θ_z-M_z}, **h** C_{3,θ_z-F_y}

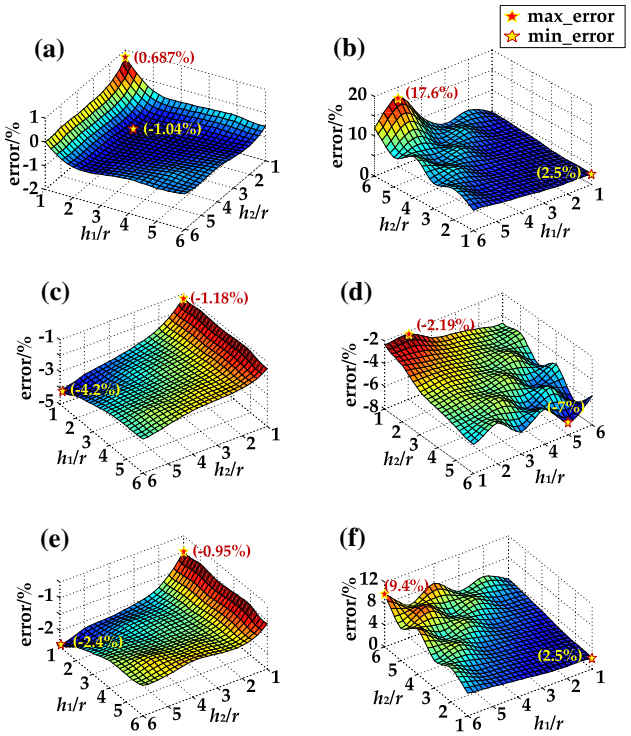

Fig. 7 Percentage relative errors between the model's predictions and FEA results for the case of $r = 5$; **a** $C_{u_x-F_x}$, **b** $C_{u_y-F_y}$, **c** $C_{u_z-F_z}$, **d** $C_{\theta_x-M_x}$, **e** $C_{\theta_y-M_y}$, $C_{u_z-M_y}$ as well as $C_{\theta_y-F_z}$ **f** $C_{\theta_z-M_z}$, $C_{u_y-M_z}$, as well as $C_{\theta_z-F_y}$

ence tends to be obvious as r increases. This is mainly because RCFH was regarded as a rectangular beam with the cross-sectional length of w and width of t.

- Models of Lobontiu and Tuo were derived using the same method (Castigliano's second theorem). Thus, they should have the same results. However, results of the linear and angular compliances for F_z are still very different. Given that Lobontiu's equations were relatively simple and the specific derivation progress was not provided, it is reasonable to guess that some approximations might have been made in his derivation.

4.2 FEA Validation

FEA is utilized as a benchmark in this section to examine the established model. FEA is conducted in ANSYS Workbench, where 3D static structure analysis method is adopted. Due to the relatively simple construction of RCFH, Design Modeler integrated in Workbench is used to model the geometry. In order to improve the computational accuracy, multi-zone sweep instead of a "smart" mesh is utilized. The material is chosen as Tc4, whose properties have been listed before. In each static analysis, the boundary conditions are chosen as: one end is fixed for all degrees of freedom, and the three-dimensional loads are applied at the midpoint of the opposite end. In addition, the loads are supposed to be ramped unit loads for the purpose of reducing the amount of calculation. The numerical simulations are carried out based on RCFHs with the width of 10 mm and thickness of 1 mm. Moreover, two new dimensionless variables h_1/r and h_2/r are utilized to quantify the relative magnitude between h_1, h_2, and r, respectively.

The percentage relative error between FEA results and analytical model's predictions is defined as $\frac{C_A - C_{FEA}}{C_{FEA}} \times 100\%$, where C_A and C_{FEA} donate for the analytical model's predictions and FEA results, respectively. The complete set of the results is plotted in Figs. 7, 8, and 9, where the cutting radius are 1, 3, and 5 mm respectively. In each case, h_1/r and h_2/r vary from 1 to 6.

It is noted that the percentage relative errors decrease with the increasing ratio of r/t. In addition, it is apparent

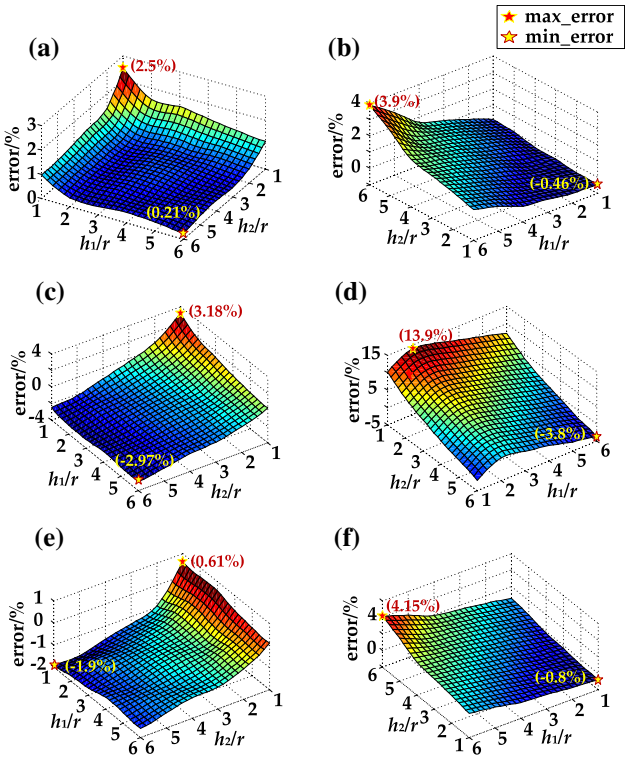

Fig. 8 Percentage relative errors between the model's predictions and FEA results for the case of $r = 3$; **a** $C_{u_x-F_x}$, **b** $C_{u_y\text{-}F_y}$, **c** $C_{u_z\text{-}F_z}$, **d** $C_{\theta_x-M_x}$, **e** $C_{\theta_y-M_y}$, $C_{u_z-M_y}$ as well as $C_{\theta_y-F_z}$ **f** $C_{\theta_z-M_z}$, $C_{u_y-M_z}$, as well as $C_{\theta_z-F_y}$

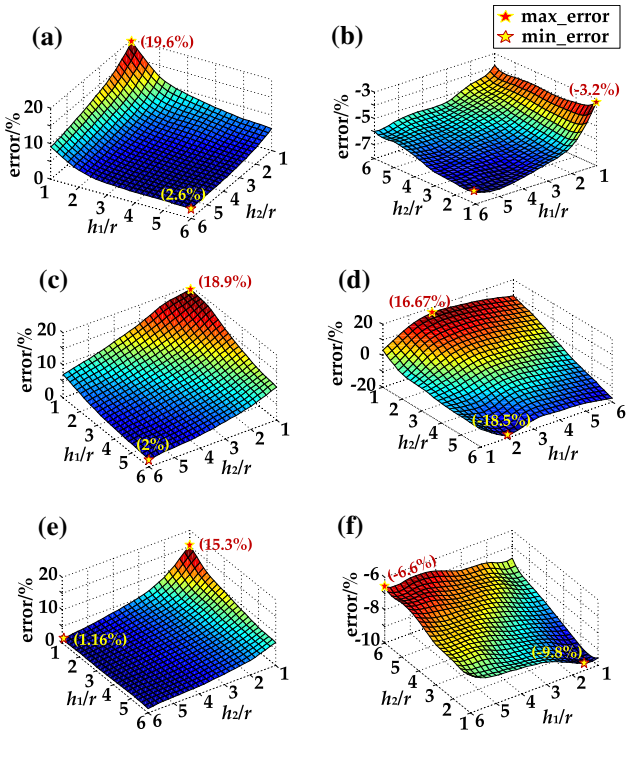

Fig. 9 Percentage relative errors between the model's predictions and FEA results for the case of $r = 1$; **a** $C_{u_x-F_x}$, **b** $C_{u_y\text{-}F_y}$, **c** $C_{u_z\text{-}F_z}$, **d** $C_{\theta_x-M_x}$, **e** $C_{\theta_y-M_y}$, $C_{u_z-M_y}$ as well as $C_{\theta_y-F_z}$, **f** $C_{\theta_z-M_z}$, $C_{u_y-M_z}$, as well as $C_{\theta_z-F_y}$

that the results between FEA and established model are in good agreement with the maximum deviation being less than 20%. This indicates the established model is accurate enough and can be used to predict RCFH's compliance during the design and optimization stage.

5 Conclusions

An analytical compliance model for RCFH has been presented in this paper, which takes the stress concentration effect into account. The stress concentration caused by changes in RCFH's cross-section is analyzed using FEA method. Relevant results show that the stress concentration will result in additional deformations and bring calculation errors on RCFH's compliance. To overcome compliance calculation errors, the stress concentration effect has been quantified during modeling RCFH's compliance. A series of closed-form equations related with geometric parameters and employed material are derived on the basis of the virtual work theory, superposition relationship of the deformation, as well as Castigliano's second theorem. Comparisons with other literatures, including Paros and Weisbord's, Wu and Zhou's, Lobontiu's, Tseytlin's, as well as Chen's, indicate the correctness of complicated definite integrals existing in these closed-form equations. FEA results and analytical predictions are found in good agreement, with maximum errors of less than 20% for a wide range of geometric dimensions. The developed model can be utilized as guidelines for RCFH as well as RCFH-based mechanism design. In addition, in order to further verify the established model, the related experiments will be conducted in our follow-up works.

Acknowledgements This research was funded by the Foundation of the National Natural Science Foundation of China (No. 61733012), the Foundation of the National Natural Science Foundation of China (No. 61703303), the Natural Science Foundation of Tianjin City (No. 17JCQNJC04100), the Project supported by State Key Laboratory of Precision Measuring Technology and Instruments (No. PILAB1705) and the Research Project of Tianjin Municipal Education Committee (No. 2017KJ086).

References

1. Lobontiu, N. (2002). *Compliant mechanisms: Design of flexure hinges*. Boca Raton: CRC Press.

2. Lobontiu, N., & Garcia, E. (2003). Two-axis flexure hinges with axially-collocated and symmetric notches. *Computers & Structures, 81*(13), 1329–1341.
3. Liu, P. B., Yan, P., Zhang, Z., & Leng, T. T. (2015). Flexure-hinges guided nano-stage for precision manipulations: Design, modeling and control. *International Journal of Precision Engineering and Manufacturing, 16*(11), 2245–2254.
4. Bhagat, U., Shirinzadeh, B., Clark, L., Chea, P., Qin, Y., Tian, Y., et al. (2014). Design and analysis of a novel flexure-based 3-DOF mechanism. *Mechanism and Machine Theory, 74,* 173–187.
5. Bhattacharya, S., Chattaraj, R., Das, M., Patra, A., Bepari, B., & Bhaumik, S. (2015). Simultaneous parametric optimization of IPMC actuator for compliant gripper. *International Journal of Precision Engineering and Manufacturing, 16*(11), 2289–2297.
6. Sattler, R., Plötz, F., Fattinger, G., & Wachutka, G. (2002). Modeling of an electrostatic torsional actuator: Demonstrated with an RF MEMS switch. *Sensors and Actuators, A: Physical, 97,* 337–346.
7. Tian, Y., Shirinzadeh, B., & Zhang, D. (2010). Closed-form compliance equations of filleted V-shaped flexure hinges for compliant mechanism design. *Precision Engineering, 34*(3), 408–418.
8. Tian, Y., Shirinzadeh, B., Zhang, D., & Zhong, Y. (2010). Three flexure hinges for compliant mechanism designs based on dimensionless graph analysis. *Precision Engineering, 34*(1), 92–100.
9. Qin, Y. D., Zhao, X., Shirinzadeh, B., Tian, Y. L., & Zhang, D. W. (2018). Closed-form modeling and analysis of an XY flexure-based nano-manipulator. *Chinese Journal of Mechanical Engineering, 31*(1), 7.
10. Wang, D. H., Yang, Q., & Dong, H. M. (2011). A monolithic compliant piezoelectric-driven microgripper: Design, modeling, and testing. *IEEE/ASME Transactions on Mechatronics, 18*(1), 138–147.
11. Wang, J., Yang, Y., Yang, R., Feng, P., & Guo, P. (2019). On the validity of compliance-based matrix method in output compliance modeling of flexure-hinge mechanism. *Precision Engineering*. https://doi.org/10.1016/j.precisioneng.2019.02.006.
12. Zettl, B., Szyszkowski, W., & Zhang, W. J. (2005). On systematic errors of two-dimensional finite element modeling of right circular planar flexure hinges. *Journal of Mechanical Design, 127*(4), 782–787.
13. Shen, Y., Chen, X., Jiang, W., & Luo, X. (2014). Spatial force-based non-prismatic beam element for static and dynamic analyses of circular flexure hinges in compliant mechanisms. *Precision Engineering, 38*(2), 311–320.
14. Zettl, B., Szyszkowski, W., & Zhang, W. J. (2005). Accurate low DOF modeling of a planar compliant mechanism with flexure hinges: The equivalent beam methodology. *Precision Engineering, 29*(2), 237–245.
15. Paros, J. M., & Weisbord, L. (1965). How to design flexure hinges. *Machine Design, 37*(27), 151–156.
16. Valentini, P. P., & Pennestrì, E. (2017). Elasto-kinematic comparison of flexure hinges undergoing large displacement. *Mechanism and Machine Theory, 110,* 50–60.
17. Yang, M., Du, Z., & Dong, W. (2016). Modeling and analysis of planar symmetric superelastic flexure hinges. *Precision Engineering, 46,* 177–183.
18. Li, Y., Xiao, S., Xi, L., & Wu, Z. (2014). Design, modeling, control and experiment for a 2-DOF compliant micro-motion stage. *International Journal of Precision Engineering and Manufacturing, 15*(4), 735–744.
19. Wu, Y., & Zhou, Z. (2002). Design calculations for flexure hinges. *Review of Scientific Instruments, 73*(8), 3101–3106.
20. Lobontiu, N., Garcia, E., & Canfield, S. (2003). Torsional stiffness of several variable rectangular cross-section flexure hinges for macro-scale and MEMS applications. *Smart Materials and Structures, 13*(1), 12–19.
21. Tseytlin, Y. M. (2002). Notch flexure hinges: An effective theory. *Review of Scientific Instruments, 73*(9), 3363–3368.
22. Yong, Y. K., Lu, T. F., & Handley, D. C. (2008). Review of circular flexure hinge design equations and derivation of empirical formulations. *Precision Engineering, 32*(2), 63–70.
23. Chen, G., & Howell, L. L. (2009). Two general solutions of torsional compliance for variable rectangular cross-section hinges in compliant mechanisms. *Precision Engineering, 33*(3), 268–274.
24. Hearn, E. J. (1997). *Mechanics of materials, 3th*. Oxford: Butterworth-Heinemann.
25. Xu, N., Dai, M., & Zhou, X. (2017). Analysis and design of symmetric notch flexure hinges. *Advances in Mechanical Engineering*. https://doi.org/10.1177/1687814017734513.
26. Li, T. M., Zhang, J. L., & Jiang, Y. (2015). Derivation of empirical compliance equations for circular flexure hinge considering the effect of stress concentration. *International Journal of Precision Engineering and Manufacturing, 16*(8), 1735–1743.
27. Awtar, S., Slocum, A. H., & Sevincer, E. (2007). Characteristics of beam-based flexure modules. *Journal of Mechanical Design, 129*(6), 625–639.
28. Linß, S., Schorr, P., & Zentner, L. (2017). General design equations for the rotational stiffness, maximal angular deflection and rotational precision of various notch flexure hinges. *Mechanical Sciences, 8*(1), 29.
29. Meng, Q. (2012). A design method for flexure-based compliant mechanisms on the basis of stiffness and stress characteristics. Doctoral dissertation, University of Bologna.
30. Young, W. C., Budynas, R. G., & Sadegh, A. M. (2002). *Roark's formulas for stress and strain*. New York: McGraw-Hill.

Weixiao Tuo received her M.S. degree from the college of precision instrument and opto-electronics engineering, Tianjin University, China, in 2017. Now she is studying for her Ph.D. degree in the college of precision instrument and opto-electronics engineering, Tianjin University. Her current research focuses on the inertial stabilized platform.

Xingfei Li is currently a professor in the college of precision instrument and opto-electronics engineering, Tianjin University, China. He received M.S. degree in instrument science and technology from Southeast University and Ph.D. degree in the college of precision instrument and opto-electronics engineering from Tianjin University, China, in 1994 and 2000. He worked as a researcher at The Hong Kong Polytechnic University, China, from 1996 to 1999 and did postdoctoral research in mechanical engineering at the University of Michigan, USA, from 2003 to 2004. His current research areas include intelligent manufacturing, inertial sensing, and ocean prediction and observation.

Yue Ji received her M.S. and Ph.D. degree in instrument science and technology from Tianjin University, China, in 2013 and 2016, respectively. She is currently a lecturer in Tianjin Polytechnic University, China. Her current research focuses on the angular velocity sensor based on magnetohydrodynamics.

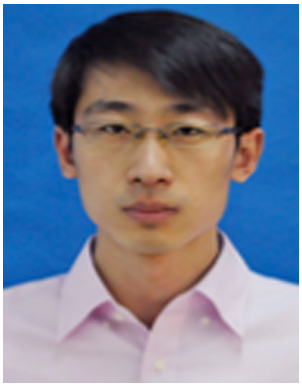

Tengfei Wu received his M.S. and Ph.D. degree in instrument science and technology from Tianjin University, China, in 2010 and 2013, respectively. Since 2014, he has been an assistant professor in Tianjin University, China. His current research interests include inertial sensing, distance measurement technology by self-mixing interferometry and LSPR sensing technology.

Ziming Xie received his M.S. degree from the Institute of electrical and electronics engineering, Tianjin University of Technology, China, in 2015. He is currently studying for his Ph.D. degree in the college of precision instrument and opto-electronics engineering, Tianjin University. His current research focuses on ocean prediction and observation.